Investigating the properties of humins foams, the porous carbonaceous materials derived from biorefinery by-products

Pierluigi Tosi, Gerard P. M. van Klink, Charlotte Hurel, Claire Lomenech, Alain Celzard, Vanessa Fierro, Clara Delgado-Sanchez, Alice Mija

Applied Materials Today 20 (2020) 100622

Contents lists available at ScienceDirect

Applied Materials Today

journal homepage: www.elsevier.com/locate/apmt

Investigating the properties of humins foams, the porous carbonaceous materials derived from biorefinery by-products

Pierluigi Tosi [a,b], Gerard P.M. van Klink [b], Charlotte Hurel [c], Claire Lomenech [c], Alain Celzard [d], Vanessa Fierro [d], Clara Delgado-Sanchez [d], Alice Mija [a,*]

[a] Université Côte d'Azur, Institut de Chimie de Nice, UMR CNRS 7272, 06108 Nice Cedex 02, France
[b] Avantium Chemicals B.V. – Zekeringstraat 29, 1014 BV Amsterdam, The Netherlands
[c] University Côte d'Azur, CNRS, Institute of Physics of Nice (INPHYNI UMR 7010), 06100 Nice, France
[d] Université de Lorraine, CNRS, IJL, 88000 Epinal, France

ARTICLE INFO

Article history:
Received 2 September 2019
Received in revised form 10 March 2020
Accepted 10 March 2020

Keywords:
Polymeric foams
Biomass valorization
Auto-crosslinking
Gas adsorption
Surface properties

ABSTRACT

Humins as biorefineries by-product can be converted with a direct heating treatment into new rigid porous carbon materials known as humins foams. Currently, not many informations about this new material are known. Here, a preparation protocol in two steps involving foaming and carbonization is reported, while the materials have been investigated in terms of morphology, elemental content, water adsorption–desorption, stability to solvents and high temperatures, and thermal conductivity. In order to evaluate their potential uses in applications such as water purification, the pH associated to the zero charge point has been identified. Foams prepared under air ventilated condition revealed an extremely negative surface, which can be used in cation exchange applications. The surface's groups have been identified by Boehm titration, showing that this behavior can be associated to the presence of acid moieties, while the basic species result absent. The humins foams have been also tested through CO_2 adsorption tests at realistic operation conditions, revealing that their performances can compete with materials reported in literature. Finally, activated carbon monoliths from carbonized humins foams using CO_2 activation were tested, reaching a surface area of 1347 $m^2 g^{-1}$ after 20 min and 1482 $m^2 g^{-1}$ after 40 min of activation. These monoliths have been characterized in terms of morphology and elemental content. The results prove that the humins foams are very versatile materials, cost effective and easy to produce, with promising properties that can be further tailored for foreseen applications.

1. Introduction

Developing research and markets around by-products has become of high interest with regards to the circular economy of industrial processes along with the environmental point of view. Often also called "industrial waste", we can identify as by-products any kind of material apart from the primary products for which the plant was originally intended. In this context, humins constitute one of the most promising by-products currently derived from the biorefinery during the conversion of lignocellulosic biomass. Humins are produced during acid-catalyzed dehydration (ACD) of C6 sugars in intermediates such as 5-hydroxymethylfurfural (HMF), alkyl derivatives (such as 5-alkoxymethyl furaldehydes: RMF), and levulinic acid (LA). Humins consist in a dark-colored material derived from random condensations between several intermediates (mainly HMF) during the ACD process [1–3]. The chemical structure of humins is mainly based on a complex network of furanic rings and aliphatic chains bearing several reactive oxygen-based functional groups (hydroxyls, ketones, aldehydes, esters, etc.) [4–6]. Due to their poor solubility and to several engineering drawbacks in their production on an industrial scale, the production of humins was considered a challenge to be overcome [9–11]. Countless the number of studies aiming to avoid the their formation [1,8,10–22]. Despite recent researches reached interesting goals in reducing the humins formation these protocols are so far limited to lab-scale methods, and unlikely to be adopted in a commercial scale plant because of technical issues, higher costs, yields and recovery challenge [21,23–29]. Therefore, as matter of fact, humins production is currently unavoidable at industrial level. Even if an industrial efficient method will be introduced, it will require further decades to be fully implemented in all the production compartments. On the other hand, the market of sustainable derived products is rising,

* Corresponding author.
E-mail address: Alice.MIJA@unice.fr (A. Mija).

https://doi.org/10.1016/j.apmt.2020.100622

and with it also the humins product. We cannot afford to consider humins as bare waste, especially considering that recent researches have proved the many hidden possibilities of this furan-rich mixture, which might in turn be attractive for the interesting properties that humins can offer [30–39].

Recently, we have reported the preparation of a new polymeric macroporous rigid material called humins foams [40], which can be obtained directly from a mixture of industrial humins by a simple one-step thermal process, without any kind of modification or pre-treatment [41]. By controlling the preparation parameters, it is possible to obtain a uniform and homogeneous porosity with adjustable cell diameters of between 0.2 and 3.6 mm, or even porosity gradients. In addition, closed/open cells yield and carbon content can be tailored by choosing the conditions of preparation. The foaming mechanism has been identified as a combination of chemical reactions and physicochemical processes taking place simultaneously. The complex viscosity of the material drops from about 2.5×10^5 Pa s to a minimum value of about 0.48 Pa s when heated from 20 to 125 °C. At this latter temperature, the matrix is sufficiently fluid to allow an easy evolution of volatile substances. From a temperature of about 140 °C, several gases, mainly low-molecular weight species produced during the heating process (e.g. H_2O, CH_3OH, CO, CO_2) are released, producing bubbles in the molten humins matrix. The hardening process occurs above 170 °C, resulting in the final porosity in the thermoset humins-based material.

However, it should be emphasized that the composition of crude humins is highly dependent from the industrial process in which they are formed, and in general they can appear in solid or viscous form. The solid material is formed when humins are collected fully crosslinked, and in this form these are barely reactive [2]. The process of humins foams production can be applied by only using humins not fully crosslinked, in the form of highly viscous mixture of oligomers [42,43]. Also in this case crude humins composition's can vary depending on the specific parameters used in the ACD of sugars. The key steps of the foaming mechanism can be subjected to small temperature differences depending on the sample used, and in particular its viscosity. However, all the samples tested gave very similar results. Thus, in general terms, it can be assumed that this mechanism represents well the humins behaviors during the foam formation process.

Given the simple and economically attractive approach of humins foams production, as well as the current market of porous polymers and carbon-based materials, this route might represent a promising valorization of humins by-products. In order to find applications for these porous materials, their physicochemical behavior, composition, thermal stability, thermal conductivity, surface chemistry and morphology should be studied in more detail. In this work, we present the results of a series of characterizations that will help future studies to promote humins foams and optimize their parameters according to the intended application. Furthermore, a preliminary test of preparation of activated carbon monoliths from humins foams has been carried out. Activated carbon preparation is a generally inexpensive way to produce valuable materials from by-products and waste [44,45]. In 2018, Kang et al. [46] reported the preparation of activated carbon from humins using chemical activation with KOH in a temperature range of 500–900 °C, reaching a BET surface area of between 428 and 1975 $m^2 g^{-1}$. Unfortunately, the material yields were quite low (15–39.2%). In the same year, Chernysheva et al. [47] reported the preparation of activated carbon from humins using KOH activation and CO_2 physical activation, but reaching a BET area of only 862 $m^2 g^{-1}$ in the best case. We decided to test the preparation of activated carbon not directly from humins but from humins foams carbonized at 900 °C, in order to use the porous rigid carbon-based structure as a whole and to produce monoliths. Unlike the conventional powder form in which activated carbon is generally available, monoliths can be easily recovered and reused and can therefore cover a wider range of applications. Herein, we have proved that it is possible to prepare materials with high surface area that can compete with those available commercially.

2. Methods

2.1. Crude materials

Humins were provided by the Avantium N.V pilot plant in Geleen (Netherlands) during the ACD of fructose into methoxymethylfurfural (MMF). This process is the key step in the production of 2,5-furandicarboxylic acid, intermediate for the production of polyethylene-furanoate (PEF).

2.2. Preparation of humins foams

The humins foams samples were designated by the letter "F" followed by the preparation temperature (e.g., F250 was prepared at 250 °C). Foams termed "F^2" were prepared with a two-step protocol (e.g., $F^2$500 was prepared by carbonizing F250 at 500 °C).

Samples F180, F220, F250 and F300 were prepared as follows: about 25 g of crude humins were installed in a rectangular flat-bottom alumina crucible and then transferred to a pre-heated Nabertherm L9/11/SKM oven for 1 h under air at temperatures of 180, 220, 250 or 300 °C, respectively. Then, the oven was set at 20 °C, and the samples were allowed to cool slowly down inside it (about 2 h required to reach room temperature).

$F^2$500, $F^2$700 and $F^2$900 were prepared by carbonization of F250 in a Carbolite GHC 12/900 tube furnace (N_2 flow ~ 80 mL min^{-1}) with the following heat treatment: heating up at 1 °C min^{-1}; isotherm 1 h at the final temperature (500, 700 and 900 °C, respectively); then 1 °C min^{-1} while cooling down to room temperature.

2.3. Elemental analysis

The elemental analysis was carried out with an Elementar Vario EL Cube analyzer. Carbon, hydrogen, nitrogen and sulfur contents were first determined by combustion of the samples at about 1700 °C (a temperature induced in a furnace, heated at 1150 °C, by a tin foil wrapping the samples and used as catalyst) in a stream of mixed oxygen and helium, the latter being used as a carrier gas. Oxygen was quantified with the same equipment in a second step, using a different procedure and another analytic column.

Headspace analysis – Headspace analyses were performed in an Agilent J&W DB624 (20 m × 0.18 mm × 1 μm) GC–MS equipped with headspace-auto-sampler and a mass-selective detector (MSD) with ionization via EI^+. 10 mg of humins or humins foams were weighed in a 20 mL vial and the vial was sealed. The vial was heated and shaken for 2 h (71 shakes min^{-1} with an acceleration of 260 cm s^{-2}) in the headspace auto-sampler, and a small amount (~1 mL) of the vapor was analyzed with GC–MS (inlet temperature 250 °C). The NIST library 11 was used for identification.

Density evaluation – Humins foams samples were cut into parallelepipeds and their volume determined accurately. The bulk density of each sample was evaluated as weight/volume (g cm^{-3}) ratio, and the average of three repetitions was calculated.

2.4. Mass titration

Three solutions of 0.2 M KCl were prepared and their pH was adjusted to either 3, 6 or 9 using 0.1 M NaOH/HCl solutions. The pH was checked at every stage using a Mettler Toledo LE pH-meter with LE438-IP67 pH electrode (calibrated every 24 h). Each of the

aforementioned solutions was used to prepare 3 sets of 6 solutions (20 mL each): 6 solutions at pH 3, 6 solutions at pH 6, and 6 solutions at pH 9. In each solution of these series, an increasing amount of milled foam was added, so that each series contained 0.05, 0.1, 0.5, 1, 5 and 10 wt.% of sample, respectively. These suspensions were stirred and their pH was measured after 24 h. The final pH of each solution was plotted against the added mass of humins foam. The pH_{PZC} can be identified as the pH to which each series tends when the sample mass increases to infinity. The results have been reported as the average of three repetitions.

2.5. pH drift method

Eight solutions of 0.02 M NaCl (13 mL each) were prepared by adjusting the pH in the range 2–9 with either 0.1 M NaOH or 0.01 M HCl solutions. The pH was checked at each step using a Mettler Toledo LE pH-meter with LE438-IP67 electrode (calibrated every 24 h). To each solution, 0.1 g of the milled foam to be studied was added, and the mixture was stirred for 24 h. The pH shift was measured at the end of the 24 h, and the results were plotted as initial pH (pH_{in}) vs final pH (pH_{fin}). The pH_{PZC} was identified by the point where the plotted curve crossed the line $pH_{in} = pH_{fin}$. The results were reported as the average of three repetitions.

2.6. Boehm titration

The number of surface oxygen-containing groups was calculated according to the Boehm titration method [48,49], using the same automatic titration equipment described in the previous subsection. 20 mL of solutions of 0.05 M NaOH, 0.05 M $NaHCO_3$, 0.05 M Na_2CO_3 and 0.05 M HCl were prepared. To each solution, 0.4 g of milled humins foams were added. The flasks were sealed and the mixtures stirred with a magnetic bar for 24 h. During this time, part of the humins surface groups was neutralized by the respective solutions. The following assumptions were considered: $NaHCO_3$ neutralizes carboxyl groups; Na_2CO_3 neutralizes carbonyls and lactones; NaOH neutralizes carboxyl/lactone/hydroxyl (phenolic) groups; HCl neutralizes all basic groups. The solutions were then filtered to remove the solid material. In order to know the amount of NaOH and HCl neutralized by the surface groups of the humins foam, 2 mL of the filtered solutions were transferred to 10 mL flasks, and titrated with 0.1 M HCl and NaOH solutions respectively. On the other hand, 2 mL of the $NaHCO_3/Na_2CO_3$ filtered solutions were transferred to a 10 mL flask; to each solution, 2 mL of 0.1 M HCl were added, and the two resulting solutions were titrated back with 0.1 M NaOH. In this case, the back-titration gives results that are more accurate. The results were checked twice by a second repetition.

2.7. Solubility test

In order to identify the species released into water, 10 g of F180, F250 and F300 humins foams were thoroughly washed with boiling distilled water (550 mL) on a Büchner funnel equipped with filter paper under vacuum pumping. The filtered solutions were collected, diluted 1/3 with distilled water and saccharin (dissolved in acetonitrile (ACN)) added as an internal standard (0.2 mg mL^{-1}). The solutions were analyzed using a Waters Acquity UPLC HSS C18 column equipped with a UV detector, using 0.2% trifluoroacetic acid in H_2O as eluent. The column was thermostated at 50 °C.

The solubility test in different solvents was carried out by adding 0.1 g of milled F250 in 20 mL of ACN, EtOH, water at pH 4, and water at pH 9.5. The flasks were then sealed and the solutions were stirred for 24 h with a magnetic bar at room temperature. After centrifugation, 1 mL of each solution was withdrawn and was diluted 1/6 with distilled water. The absorbance of the resultant solutions was acquired using a SHIMADZU UV-1800 spectrometer between 200 and 800 nm.

2.8. Thermal conductivity

The thermal conductivity was measured from parallelepiped-cut samples of humins foams (minimum dimensions 3 × 3 × 2 cm) using the transient plane source method with a Hot Disk TPS 2500 S thermal conductivity analyzer under fixed conditions of temperature and moisture content (20 °C and 40% relative humidity).

2.9. Thermal stability and mass loss analyses

Thermal stability and mass loss of humins foams were investigated by thermogravimetric analysis (TGA) using a Mettler Toledo TGA/SDTD 851 with a microbalance accuracy of ±0.1 μg. The data were analyzed with STAR© software. Milled humins foams (10–12 mg) were placed in a 70 μL alumina pan and submitted to dynamic thermal programs. The thermal stability was evaluated between 25 and 1000 °C with a heating rate of 10 °C min^{-1} (air flow = 80 mL min^{-1}), and was reported as the T_{10} value, corresponding to the temperature at which 10% of the mass was lost. The results were then averaged over two replicates.

2.10. Water vapor adsorption

Water vapor sorption–desorption isotherms were obtained with a Micromeritics 3Flex automatic device. Prior to analysis, the samples were outgassed under secondary vacuum at 110 °C for at least 72 h. The sorption measurements were performed by dosing water vapor at relative pressures (P/P_0) ranging from 1% to 90% at 20 °C, and measuring the equilibrium sorbed water for each value of P/P_0. Once P/P_0 = 90% was reached, desorption was monitored, and the corresponding equilibrium sorbed water volumes were measured to build the desorption branch.

2.11. N_2 and CO_2 adsorption

Nitrogen (N_2) and carbon dioxide (CO_2) adsorption isotherms at −196 and 0 °C, respectively, were obtained with ASAP 2020 and ASAP 2420 (Micromeritics) automatic adsorption devices, respectively. The samples were outgassed under vacuum prior to adsorption analysis for at least 48 h at 110 °C.

Using Microactive® and SAIEUS® software provided by Micromeritics, the following parameters were calculated: (i) BET area, A_{BET} ($m^2\ g^{-1}$), using the Brunauer–Emmet–Teller method [50]; (ii) total pore volume, $V_{0.92,N_2}$ ($cm^3\ g^{-1}$) or Gurvitch volume, taken as adsorbed volume at the relative N_2 pressure of 0.97; (iii) Dubinin micropore volume, $V_{DR\text{-}N2}$ *or* $V_{DR\text{-}CO2}$ ($cm^3\ g^{-1}$), from the Dubinin–Raduskevich method applied to the N_2 or CO_2 isotherms, respectively; (iv) specific surface area and micropore volume by applying the *dual gas analysis method* (2D-NLDFT) method to N_2 and CO_2 isotherms, S_{NLDFT} ($m^2\ g^{-1}$) and $V_{\mu,NLDFT}$ ($cm^3\ g^{-1}$), respectively [51,52]. An improved version of the 2D-NLDFT method, which takes into account the diffusion limitation in ultramicropores, was applied [53]. The pore size distribution (PSD) was also determined by applying the 2D-NLDFT to the calculation of: ultramicropore volume (pore size less than 0.7 nm) $V_{<0.7,NLDFT}$ ($cm^3\ g^{-1}$), supermicropore volume (pore size between 0.7 and 2 nm) $V_{0.7\text{–}2,NLDFT}$ ($cm^3\ g^{-1}$), micropore volume $V_{micro,NLDFT}$ ($cm^3\ g^{-1}$), total pore volume $V_{T,NLDFT}$ ($cm^3\ g^{-1}$), and average pore volume w_{av} (nm).

2.12. CO_2 adsorption above room temperature

22 mg of milled humins foams were placed in a platinum crucible with a pierced lid. The samples were analyzed with TGA under

a gas flow of 80 mL min^{-1} using the following program: from 25 to 120 °C at 30 °C min^{-1} under N_2 (necessary to remove all gases previously adsorbed); isotherm of 30 min at 120 °C under N_2; cooling to the temperature of experiment (25/50/70/100 °C) at 30 °C min^{-1} under N_2; equilibrium of 30 min under N_2. At this point, the gas was switched to CO_2 and the weight change was recorded for 1 h. The adsorbed CO_2 is expressed in wt.% relative to the mass of the sample. The saturation of the CO_2 adsorption, corresponding to the point where no additional CO_2 can be adsorbed on the surface of the humins foam is observed where the increase of the mass in the thermograph reaches the plateau, and is expressed in minutes.

2.13. Tap density determination

Tap and bulk density of F²900 was measured with the tapped density analyser AUTOTAP (Quantachrome Instruments) and following the ASTM D8176-18 standard test method [54].

2.14. Preparation of activated carbon

Approximately 250 mg of block F²900 sample was weighted accurately and placed in an alumina crucible. Then, the sample was placed in a tubular quartz furnace. The sample was heated to 900 °C under N_2 (60 mL min^{-1}) at 5 °C min^{-1}. Then, the gas was switched to CO_2 (60 mL min^{-1}) and held at 900 °C for the selected activation time (10, 20, 40 or 60 min). Finally, the gas was switched back to N_2, and the furnace was allowed to cool to room temperature.

3. Results and discussion

3.1. Porous structure and composition

Crude humins directly collected at the industrial plant and without any purification or modification step can be auto-crosslinked and foamed by a direct thermal activation process. However, the control of both the porosity and the morphology of the final foam requires the optimization of all the parameters involved (heating ramp, final temperature of the treatment, nature of the mold, etc.). For instance, using a heating rate of 1 °C min^{-1} in a tubular oven under a flow of N_2, no foam is produced but a completely flat material is obtained instead. The chemical reactions and the gas evolution dynamics are indeed so slow that not enough bubbles are produced, and there remains after curing a quite low porosity in the material. Furthermore, ordinary tubular furnaces used for carbonization can only operate with limited amounts of material, whereas the nature of the available crucibles is generally restricted to ceramics.

To better control porosity and foaming yield, a two-step preparation is suggested. The first heating step can be carried out in air in any kind of oven using temperatures below 350 °C. Under these conditions, any type of mold, crucible, amount of humins and heating ramp can be easily applied without constraints (e.g. 1 kg of crude humins in aluminum pans). In this way, it is possible to produce large amount of humins foams in a short time, while the temperature can be adjusted according to the desired porosity. Afterwards, the as-prepared humins foams can be carbonized at any selected temperature under N_2 and, as they have been thermoset in the previous step, the heating rate used during the carbonization does not influence the porosity.

Based on this procedure, we studied the effect of this 2-step treatment on industrial humins and the main results concerning the synthesis yield and the characteristics of the process are presented in Table 1. The samples called F250 has been prepared from crude humins through a 1-step treatment at 250 °C (Fig. 1), while F²500 and F²900 (2nd step) have been prepared from F250 by carbonization at 1 °C min^{-1} from 25 to 500 °C and to 900 °C, respectively.

One hour of isothermal direct treatment at 250 °C resulted in a final foam F250 with a volume 345% higher than that of the starting crude humins. During this process, a mass loss of about 20% was observed, which is slightly lower than that reported in our previous work [55] due to a different thermal program (here, a direct isothermal treatment instead of a dynamic heating ramp). This method was carried out in the temperature range corresponding to the first step of mass loss deduced from the TGA of humins (140 and 260 °C).

Table 1
Data related to the preparation of humins foams, in 1 or 2 steps. The yields of the last step indicate the preparation yield for F250 (single step), and the carbonization yield for F²500 and F²900.

	Yield of last step (wt.%)	Total yield (wt.%)	Foaming capacity (vol.%)	Shrinkage (from F250) (vol.%)	Bulk density (g cm^{-3})
F250	78–80	78–80	345	–	0.055
F²500	50–52	41–43	290	17	0.070
F²900	45.5–47.5	36–37	265	23	0.092

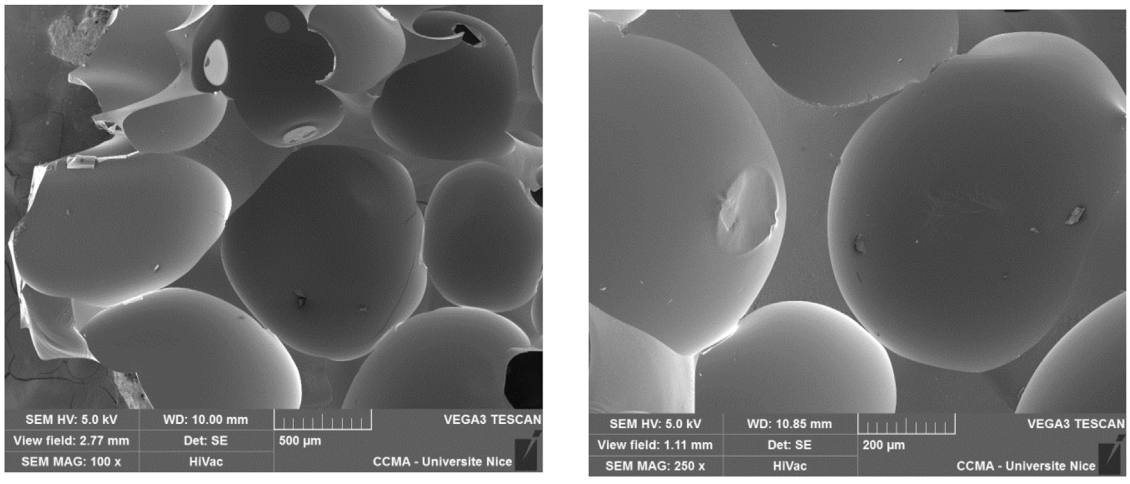

Fig. 1. SEM images of F250 humins foam.

Table 2
Textural characterization from N_2 and CO_2 adsorption data at −196 and 0 °C, respectively, for all materials tested.

	N_2			CO_2		$N_2 + CO_2$				
	A_{BET} (m^2/g)	$V_{DR\text{-}N2}$ (cm^3/g)	$V_{0.97}$ (cm^3/g)	A_{BET} (m^2/g)	$V_{DR\text{-}CO2}$ (cm^3/g)	S_{NLDFT} (m^2/g)	$V_{<0.7,NLDFT}$ (cm^3/g)	$V_{0.7\text{-}2,NLDFT}$ (cm^3/g)	$V_{micro,NLDFT}$ (cm^3/g)	$V_{Total,NLDFT}$ (cm^3/g)
F250	–	–	0.00		–	–	–	–	–	–
F²500	–	–	0.01	224	0.18	493	0.12	0.02	0.14	0.14
F²700	–	–	0.01	328	0.33	756	0.17	0.02	0.19	0.19
F²800	736	0.28	0.29	445	0.33	893	0.16	0.14	0.30	0.30
F²900	837	0.31	0.33	477	0.26	970	0.14	0.19	0.33	0.33
F²1000	711	0.27	0.28	481	0.28	930	0.18	0.14	0.32	0.32

According to TGA-MS analysis, it was associated with the release of low-molecular weight species (mainly H_2O, CO_2, CO and MeOH) [55]. Although TGA-MS was unable to detect any other volatile compound emitted by the material during thermal crosslinking, headspace analysis of the crude humins evidenced the presence of other species, especially furanic compounds. Head-space analyses were performed on crude humins at 170 °C (slightly below the hardening temperature), and are consistent with previously reported results [38]. During this heating process, 16% of the total mass loss of the untreated sample was found in TGA, corresponding to the release of volatile compounds present in industrial humins. These species contribute mainly to the emission of gases during the heat treatment of humins, leading to the formation of cells in the final porous thermoset. According to headspace analysis, of these 16% of mass loss, only about 7.9% were furanic compounds, mainly unreacted molecules derived from the ACD process and trapped in the matrix.

According to the characterization of the surface texture (BET and NLDFT) indicated in Table 2, the foam F250 has a negligible surface area, since the heat treatment was too mild to produce porosity. In contrast, the foam F²500, obtained by carbonization under N_2 of F250 at 500 °C, presented a mass loss of approximately 50% during its preparation and made it possible to obtain a final yield of about 42%. In this case, the foaming capacity was lower than that of the starting sample F250, i.e., with a volume 290% higher than that of the initial crude humins. This is due to thermally induced rearrangements of the polymer network and the aromatization of the structure shown by the FT-IR analysis [55], which led to a 17% shrinkage of F²500 compared to F250, without modifying the global morphology. Again, the surface area of this foam remained little changed since the temperature was too low to produce additional porosity.

As in the previous case, the foam F²900 was prepared by carbonization under N_2 of F250 at 900 °C. During this step, the material loses a mass fraction about 55% higher than the starting F250, which gives a final yield of about 36%. Due to the higher temperature, the shrinkage was higher than that of F500 (23%), giving a foam volume 265% higher than that of the starting crude humins.

In terms of BET area (A_{BET}) humins foams do not have a large surface area [56]. However, when the surface area was calculated by the 2D-NLDFT method, S_{NLDFT}, assuming slit pores, the result was higher than expected, reaching values of 756 and 970 $m^2\ g^{-1}$ after carbonization at 500 and 900 °C, respectively. The surface area of F²900 is thus particularly high compared to that measured for tannin-derived carbon foams, always lower than 1 $m^2\ g^{-1}$ [57,58]. The higher value of S_{NLDFT} when compared to A_{BET} is due to the existence of very narrow porosity, which is only accessible to CO_2 at 0 °C or in which only a monolayer of nitrogen can penetrate. In this sense, the application of the refined 2D-NLDFT model, developed for the analysis of biochars [53], confirmed that the best simultaneous fitting of N_2 and CO_2 isotherms was obtained when the lower limit of pore width, w_{min}, of the N_2 kernel was 4.6 nm and not 3.6 nm. The adjustable value of w_{min} has a physical meaning as it provides an estimate of the minimum pore width accessible to N_2 molecules in the present conditions of measurement. Fig. 2 shows the good simultaneous fit of N_2 and CO_2 isotherms and the corresponding pore-size distribution (PSD) obtained from this fit. The PSD showed that the carbon foam was exclusively microporous, with an average pore diameter of 0.78 nm. For F²900, more than half of the microporosity corresponded to ultramicropores, $V_{0.7,NLDFT} = 0.16\ cm^3\ g^{-1}$, while the total micropore volume was $V_{micro,NLDFT} = 0.30\ cm^3\ g^{-1}$. The total volume calculated by the 2-NLDFT model was higher than that determined by N_2 adsorption, due to nitrogen diffusion limitations at −196 °C. This also agrees with the higher micropore volume of F²900 determined by DR method from CO_2 adsorption data, $V_{DR\text{-}CO2}$, compared to that deter-

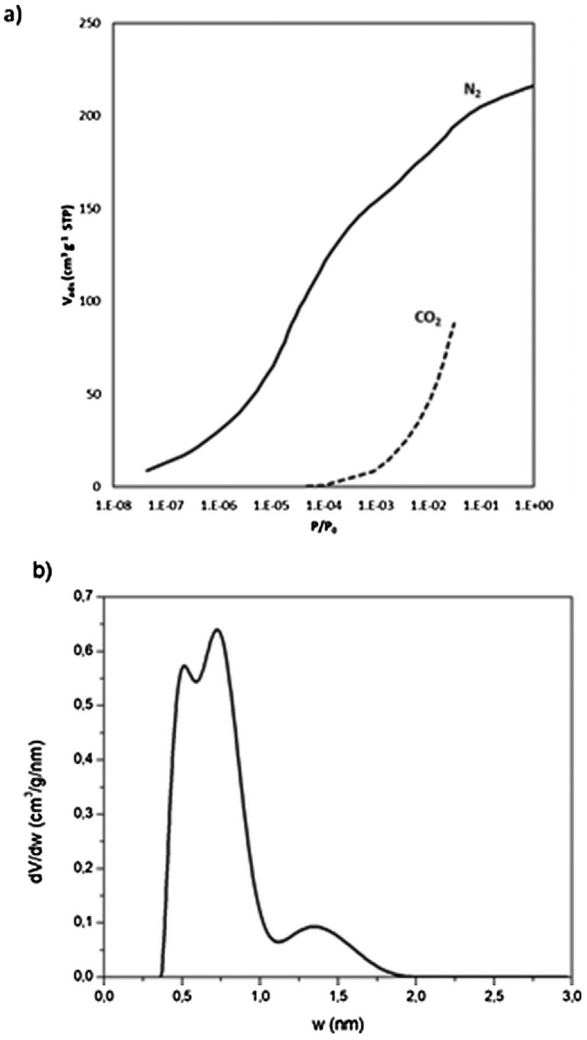

Fig. 2. (a) Simultaneous fit of both N_2 and CO_2 isotherms of the F²900 foam by the refined 2D-NLDFT-HS method (the lines represent the predictions of the model); and (b) pore-size distribution obtained by application of the 2D-NLDFT method.

Table 3
Elemental analysis of humins foams.

Sample	C (wt.%)	H (wt.%)	O (wt.%)	N (wt.%)
F250	61.25	4.70	34.56	0.06
F^{2}400	74.45	3.50	23.02	0.08
F^{2}500	84.25	3.10	12.20	0.13
F^{2}600	89.95	2.20	6.01	0.26
F^{2}700	93.20	1.20	6.25	0.48
F^{2}900	94.28	0.75	5.60	0.39
F^{2}1000	96.06	0.19	1.24	0.29

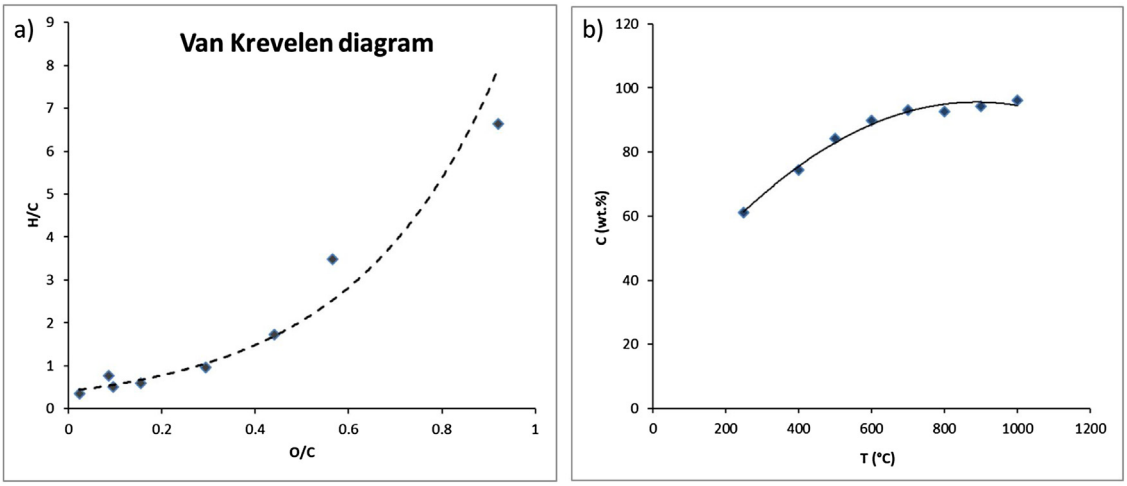

Fig. 3. (a) Van Krevelen diagram and (b) evolution of carbon content as a function of temperature for the carbonization of humins foams.

mined from N_2 adsorption data, $V_{DR\text{-}N2}$. Therefore, the presence of narrow ultramicropores with pore diameters of less than 0.5 nm, where diffusional resistances of nitrogen at −196 °C are important, makes $S_{NLDFT} > A_{BET}$, $V_{DR\text{-}CO2} > V_{DR\text{-}N2}$, and $V_{T,NLDFT} > V_{0.97}$.

In terms of macroporosity, according to our observations, the carbonization steps of F250 at 500 °C (in the preparation of F^{2}500) and 900 °C (in the preparation of F^{2}900) had a minor impact on the porous structure, the shape of the cells shape or the general aspect of the foams. F250 had indeed a homogeneous and uniform macroporosity, with pore diameters between 0.5 and 0.7 mm, while the cells were closed (Fig. 1). These properties were maintained in the derived foams obtained by carbonization at 500 and 900 °C, except for the corresponding shrinkage, which slightly reduced the pore diameters (0.3–0.5 mm in F^{2}900). Such shrinkage did not alter the shape of the material but only reduced its size. Indeed, carbonizing F250 parallelepipeds to 500 and 900 °C led to smaller final samples but maintaining exactly the same proportions.

The bulk density of the foams increases with the carbonization temperature, from 0.055 g cm^{-3} for F250, to 0.070 g cm^{-3} for F^{2}500, and 0.092 g cm^{-3} for F^{2}900 (Table 1). This effect is due to both the shrinkage/aromatization and the corresponding increase of carbon content.

Indeed, in terms of elemental content, as can be seen from the elemental analysis (Table 3) and the van Krevelen diagram (Fig. 3), the increase in the carbonization temperature of humins foams leads to a higher and higher carbon content, while the oxygen is gradually eliminated. From a C content of 53 wt.% in crude humins, it was possible to reach about 90% of C with a carbonization temperature of 600 °C. A maximum C content of 96% was reached in case of carbonization at 1000 °C, which corresponds to an almost pure carbon material. In this case, the residual O is only around 1.2 wt.%. These carbon foams are electrically conductive materials that could find application in several fields (e.g., in the preparation of sacrificial electrodes, electrical devices, supercapacitators) or as microwave absorbers and shields for electromagnetic protection.

The water adsorption data at 25 °C of materials F250, F^{2}500 and F^{2}900 are shown in Fig. 4. The first part of the water adsorption isotherm, i.e., at $P/P_0 < 0.3$, reveals affinity of materials for water and is closely related to the nature and the amount of surface functional groups. The slope of the isotherm at $P/P_0 < 0.3$ decreased in the order F250 > F^{2}500 > F^{2}700 > F^{2}900, indicating the removal of oxygenated groups at increasing temperature, in agreement with the elemental analysis (Table 3). The second part of the water adsorption isotherm is related to the surface area, and hence the maximum amount of adsorbed water decreased in the order F^{2}900 > F^{2}700 > F^{2}250 > F^{2}500, in good agreement with the results obtained by N_2 and CO_2 adsorption already reported in Table 2. The maximum water uptake of 27.6 wt.% corresponds to F^{2}900 at $P/P_0 = 0.92$.

3.2. Surface chemistry

During the foaming process of humins, the O content can be adjusted with the C content, which provides a good indication of the surface reactivity of the material. As shown in Table 3, the O content decreased from 34.5 wt.% in F250 to about 12 wt.% in F^{2}500, and even to 5.6 wt.% in F^{2}900. The minimum was found for F^{2}1000, with only 1.2 wt.% of oxygen. Such a decrease in the amount of oxygen species was expected during the carbonization step. However, since some of this oxygen content can be involved in residual furan rings or in moieties of the crosslinked structure (such as ether, ester or ketone groups in the bulk), it is not possible to evaluate the surface behavior of these materials only based on this information.

By studying the oxygenated functions present on the surface of the material, useful information can be obtained concerning the possible applications of humins foams, such as adsorbents for water treatment or catalyst supports. In this context, one of the most important parameters describing the variable surface charge is the point of zero charge (PZC), which is the pH that an aqueous solu-

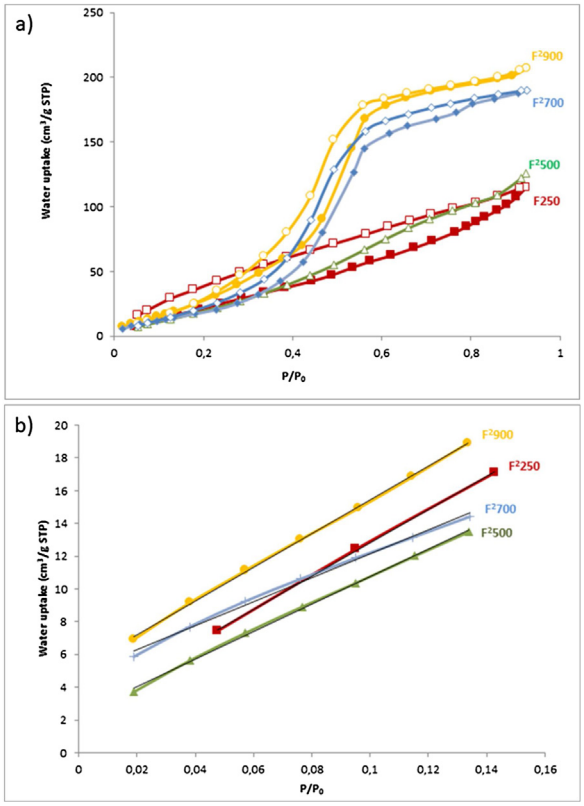

Fig. 4. Water adsorption–desorption isotherms of humins foams F250, F2500, F2700 and F2900: (a) complete data set; (b) zoom on the range of low relative pressures.

tion in which the material is immersed must have to produce a total surface charge equal to zero (neutrality) [59]. When the material is immersed in a solution whose pH is above the PZC, its surface has a net negative charge and therefore has a cation-exchange capacity (CEC). If the same material is immersed in a solution whose pH is below its PZC, it has a net positive charge with the ability to retain anions electrostatically, i.e., it has an anion-exchange capacity (AEC). To determine the PZC, several methods can be used, which may cause slight differences, depending on the technique.

The pH drift test is a method generally used to evaluate the PZC of a series of similar materials [60,61]. In this method, a certain amount of milled sample is added to an aqueous solution of known pH, and the variation of pH is recorded so that a curve of the initial pH (pH_{in}) with respect to the final pH (pH_{fin}) can be built. The PZC is thus obtained as the intersection between the resultant curve pH_{in} vs. pH_{fin} and the line $pH_{in} = pH_{fin}$. Another method is the mass titration method [62,63], initially developed for OH-rich surfaces. The method is based on the principle that, by adding more and more solid to a solution of known pH, the latter will tend toward a pH limit value corresponding to the PZC. Therefore, starting from 3 solutions with different initial pH, and adding to each of them an increasing amount of solid, it is possible to build 3 pH curves that tend to the same value corresponding to the PZC of the solid. However, this method has some disadvantages, because the exact value associated to pH with a mass material tending to infinity is not always well defined (the curves sometimes tend toward slightly different pH), and the technique is theoretically limited to samples free of impurities. However, we used it to recheck the previous values obtained by the pH drift method. Humins foams prepared at low temperature (F180, F250 and F300, respectively prepared at 180, 250 and 300 °C under air) were also tested. Despite the good agreement found between the two techniques when using these foams, fluctuations were noted for F^2500 and F^2900.

Table 4
PZC obtained from different techniques.

Sample	pH drift method	mass titration
F180	1.98	2.0
F250	2.0	2.0
F300	2.0	2.02
F^2500	6.6	7.2
F^2900	7.9	6.8

The results obtained are reported in Table 4. They show that F180, F250 and F300 foams have a net negative acidic surface, with a notable value of PZC of about 2. This means that the surface of these foams is negative when immersed in water with pH values above 2, and is positive only under extreme acidic conditions, with a water pH below 2. Since, in common aqueous applications, the pH usually ranges between 4 and 10, it can be assumed that the surfaces of F180, F250 and F300 are always negatively charged. On the other hand, the values obtained for F^2500 and F^2900 with pH drift and mass titration methods show some discrepancies, but within the limit of one pH unit. We can however approximate for both samples a PZC of around 7. According to these results, carbonization at 500 °C under inert atmosphere (N_2) is already able to produce a neutral surface by removing oxygen-based moieties from the surface, in agreement with the elemental analysis. In contrast, the PZC obtained for foams treated at lower temperatures (F180, F250 and F300) in air (oxidizing conditions) are extremely promising in CEC applications.

In order to better understand the nature of the remarkably low PZC values of F180, F250 and F300, the Boehm titration method [48,49,64,65] was used on a milled F250 foam. The results are reported in Table 5.

Boehm's titration method is commonly used to identify and quantify oxygen-based functional groups on the surface of porous materials [49,64–68]. The technique is based on the assumption that bases/acids of given strengths can only neutralize stronger acids/bases. Therefore, it is assumed that $NaHCO_3$ ($pK_{NaHCO3} = 6.37$) can only neutralize carboxyl groups, that Na_2CO_3 ($pK_{Na2CO3} = 10.25$) neutralizes carbonyls and lactones, while NaOH ($pK_{NaOH} = 15.74$) neutralizes all the acidic groups of the surface (carboxyls, lactones and hydroxyls). The total amount of basic surface groups can be evaluated by titration with a strong acid such as HCl. According to the results, the surface acidity of F250 can be justified by the presence of carboxylic acidic groups on the surface, accompanied by the total absence of basic sites. The main moieties present are OH-groups, while lactones are present only in the form of traces.

Since the PZC of foams prepared between 180 °C (minimum foaming temperature) and 300 °C is the same, it can be assumed that the chemical moieties on the surface of these materials are also very similar. These surprisingly low PZC values suggest their potential application to depollution of water by CEC effect.

3.3. Chemical stability

From the economical, practical and ecological point of view, the most interesting foam is the one that can be prepared at the lowest temperature (F180). However, since the chemical and thermal stability of such materials is influenced by the temperature of preparation itself, we must evaluate this aspect in order to identify the minimum preparation temperature of foam samples that can be applied in contact with solvents.

To evaluate the chemical stability of humins foams, samples of F180, F250 and F300 were milled and washed extensively with boiling distilled water, and the washings were analyzed by UPLC and GC–MS. While F250 and F300 wash solutions were clear and no dissolved species found inside, confirming the good stability of these

Table 5
Boehm titration results for F250 humins foam.

Sample	A_{BET}	Carboxylic groups		Lactonic groups		Hydroxyl groups		Basic groups		Total acidic groups	
	$m^2\ g^{-1}$	mmol g^{-1}	mmol m^{-2}	mmol g^{-1}	mmol m^{-2}	mmol g^{-1}	mmol m^{-2}	mmol g^{-1}	mmol m^{-2}	mmol g^{-1}	mmol m^{-2}
F250	0.2	0.2	0.9	0.09	0.3	0.4	1.6	0	0	0.7	2.8

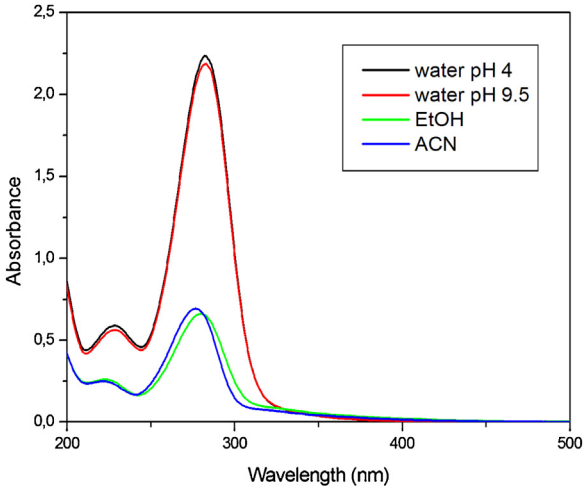

Fig. 5. UV–vis absorbance spectra of foam F180 washing solutions using ethanol (EtOH), acetonitrile (ACN), or water at different pH (4 and 9.5).

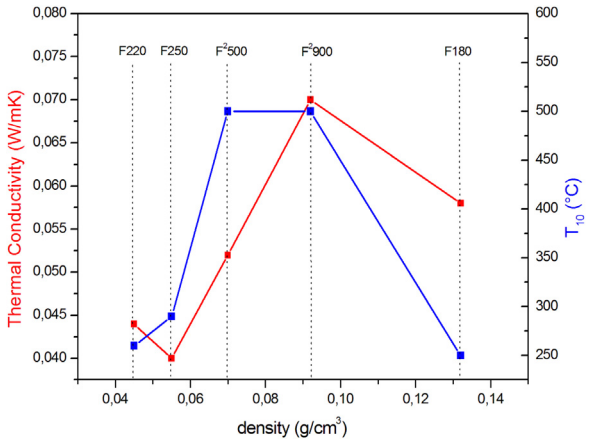

Fig. 6. Thermal conductivity and T_{10} values (derived from TGA at 10 °C min^{-1} between 25 and 1000 °C under 50 mL min^{-1} air flow) as a function of the bulk density (ρ) of 5 samples of humins foam.

foams, the resultant solution from F180 had an intense yellowish color. Furanic species were found in this solution by UPLC analysis, leading to the conclusion that F180 is not chemically stable. This can be explained by incomplete crosslinking of the structure at 180 °C, leading to the release of monomers or small oligomeric species.

Additional solubility tests were carried out by adding 0.1 g of milled humins foams to 15 mL of different solutions (water at pH 4, water at pH 9.5, EtOH, acetonitrile) and stirring the obtained suspensions for 24 h. Again, F250 and F300 demonstrated good stability, since no soluble species was found in the corresponding filtered solutions. On the other hand, the presence of furanics dissolved in F180 washing solutions was observed by UV–vis spectroscopy (Fig. 5). 180 °C is here confirmed to be a too low temperature to allow complete crosslinking of humins. The species released could come from either (i) small molecules released by hydrolysis from the surface of the foams, or (ii) unbounded furanic species trapped in the humins mixture during the ACD process of sugars. Furthermore, according to headspace analysis, the treatment of F180 at 250 °C causes a loss of mass of 8.5%, of which 4.2 wt.% comes from furanic compounds released in the form of volatiles. This can further justify the absence of these compounds in F250, where all volatiles are released at a higher foam preparation temperature. According to these results, it is not recommended to use F180 in applications involving immersion in solutions. However, F250 has shown good chemical stability, so the minimum temperature for preparing a stable foam for such applications can be set at 250 °C.

3.4. Thermal behavior

The thermal conductivity, the bulk density (ρ) and the value of T_{10}, i.e., the temperature at which the material loses 10% of its mass, of several humins foams are reported in Fig. 6. It can be seen that F180 has a much higher density (0.132 g cm^{-3}) than that of other humins foams (below 0.1 g cm^{-3}). Indeed, 180 °C does not provide a sufficient mass loss (only 5.5 wt.% with a ramp of 10 °C min^{-1}), so that little gas is emitted during the preparation, which leads to a lower porosity in the final material. By using higher temperatures of 220 °C (mass loss of 12 wt.%) and 250 °C (mass loss of 20 wt.%), foams F220 and F250 are produced respectively with lower density and lower thermal conductivity. A further increase in the preparation temperature results in an increase in the density of the foams due to shrinkage, as well as an increase in the thermal conductivity due to aromatization and increased C content. The maximum value of thermal conductivity was found for $F^2$900, 0.070 W m^{-1} K^{-1}, as predicted by its elemental composition (almost pure carbon) and its higher density (0.092 g cm^3). After optimization, foams F220, F250 and $F^2$500 might find interesting applications as thermal insulating materials. Indeed, according to the Federation of European Rigid Polyurethane Foams Associations, a material can be considered as good insulator if its thermal conductivity is in the range 0.035–0.055 W m^{-1} K^{-1} [69].

On the other hand, the T_{10} value can be used to evaluate the thermal stability of humins foams. In unreacted crude humins, T_{10} was found to be around 200 °C [55], whereas this value is higher in humins foams. With regard to the latter, T_{10} increases with the preparation temperature. This result was expected, since once a given temperature is reached during the preparation of the foam, all the possible reactions that can occur at this temperature are performed. New reactions, and therefore new loss of mass, can be observed only when the temperature is further increased. Thus, for instance, when the F300 foam is prepared at 300 °C, we assume that all the processes that could have happened at a lower temperature (e.g. 100, 150, 200, 250 °C) have already occurred, and that no mass loss can be observed below 300 °C.

The maximum value of T_{10} was reached with $F^2$500 (T_{10} = 500 °C), which corresponds to the value at which thermo-oxidative degradation (pyrolysis) occurs completely in air under the conditions used here. Above 500 °C, the material burnt completely. Thus, under air, no higher thermal stability can be achieved for humins foams using dynamic heating of 10 °C min^{-1}, as used in this work.

To further evaluate the thermal stability of humins foams, headspace analyses of F180, F250 and F300 were carried out. Although these results were obtained by a qualitative analysis, we

attempted to get semi-quantitative data using the total mass loss of the sample obtained by TGA and the comparisons between the areas of signals peaks in GC–MS. These results provide additional information about the nature of the gases emitted when humins foams are subjected to heating processes or thermal sources.

F180 already releases gases at 100 °C, with a mass loss of 0.5%. Of these gases, about 70% (corresponding to about 0.35% of the total mass lost by F180 at 100 °C) corresponds to furanic compounds, while about 23.6%, corresponding to 0.12% of the total mass of F180, is associated with degradation compounds (i.e., acetone, MeOH and acetic acid).

By increasing the F180 treatment temperature, new unknown signals were found in the chromatogram. A possible candidate might be 5-methoxyfuran-2-carbaldehyde, not present in our library. As expected, the highest temperature investigated (250 °C) gave the largest amount of gas emitted by F180, which corresponds in any case to only 8.5% of the total mass of F180. The maximum signal for F180 at 250 °C is associated with furanic compounds, which correspond to only about 4.21% of the mass released by F180 in 2 h. Specifically, and according to TGA, this mass loss occurs within the first 45 min, after which no further mass loss is detected, regardless of the duration of the thermal treatment. Therefore, we can conclude that no hazards are associated with F180 during similar thermal events.

As expected, the other foams studied (prepared at higher temperatures) showed greater thermal stability. No species was emitted and detected by treatment of F250 and F300 to 100 and 150 °C. At 200 °C, F250 had a mass loss of less than 1%, mainly associated with degradation products. The loss of mass detected for F300 was even lower, and no furanics could be identified, suggesting their complete release during the foam preparation at 300 °C. Headspace analysis of F300 at 200 °C identified water as the main released compound, which can either be a residual by-product of condensation reactions or originate from water formerly adsorbed from the environment. Acetic acid was the main degradation product found for F300 at 250 °C. At the same temperature, traces of 2,3-butadiene and 2-butanone also appeared as degradation products, possibly associated with the higher carbon content of F300. These values are mainly relevant for describing trends. However, considering these values being the result of an overestimation, we envisage the worst possible scenario of evolution of volatiles. In the case where humins foams would be accidentally subjected to thermal sources, we can foresee an extremely limited risk for the environment and human health, in agreement with the previously reported studies [70,71].

3.5. CO_2 adsorption

The application of humins foams to the adsorption of CO_2 at a temperature higher than or equal to room temperature has been tested, and the results are presented in Table 6. CO_2 is a molecule that can be easily adsorbed in materials having micro- and ultramicropores. Due to its low surface area (Table 2), F250, has the worst performance in terms of CO_2 adsorption. F^{2}500 and F^{2}700 adsorb more CO_2, and in a faster way. The fastest adsorption was observed for F^{2}500, where saturation was observed after only 37 min at 25 °C, while the largest amount of adsorbed CO_2 was found for F^{2}700, with 3.66 wt.% of CO_2 adsorbed. By increasing the temperature, the adsorbed molecules are less and less retained in the porous materials. F^{2}900 presented a quite high adsorption capacity, although less than the previous cases, its best value being 2.64 wt.% of CO_2 adsorbed at 25 °C. These results are comparable with those reported for material studied for similar application, with the advantage that humins foams are completely bioderived and that no surface activation have been performed [72].

Table 6
CO_2 adsorption capacity of humins foams F250, F^{2}500, F^{2}700 and F^{2}900 at different temperatures (25, 50, 70 and 100 °C). The saturation of the surface, expressed in time, is found when one reaches the plateau of the thermogram under flow of CO_2 gas.

	Temperature	CO_2 adsorbed (wt.%)	Saturation (min)
F250	25 °C/298 K	0.52	>60
	50 °C/323 K	0.38	>60
	75 °C/348 K	0.25	>60
	100 °C/373 K	0.17	46
F^{2}500	25 °C/298 K	2.61	37
	50 °C/323 K	1.47	25
	75 °C/348 K	0.80	19
	100 °C/373 K	0.43	14
F^{2}700	25 °C/298 K	3.66	44
	50 °C/323 K	3.10	42
	75 °C/348 K	2.02	36
	100 °C/373 K	1.23	29
F^{2}900	25 °C/298 K	2.64	>60
	50 °C/323 K	2.56	>60
	75 °C/348 K	1.77	>60
	100 °C/373 K	1.17	>60

Table 7
Tap density obtained with Autotap analyzer.

	F^{2}900 (AUTOTAP)
Mass	4.849 g
Volume	4.85 mL
Tap density	1.00 g cm^{-3}

Furthermore, we also found an almost perfect correlation between the differences in CO_2 adsorption at 50 and 100 °C and the volumes of micropores (<1 nm) calculated by NLDFT (SI 1 and SI 2). This confirms that CO_2 adsorption involves mainly pores with volumes minor than 1 nm.

The capacity of storage at high temperatures (100 °C), which is relevant for combustion gases, can be compared in literature with results for similar materials. Relevant data have been recently reported about activated anthracite MSP-20X of KANSAI Coke (Japan) [73]. Compared to humins foams, the latter carbon material has a higher surface area (A_{BET} = 2363 m^2 g^{-1}). Its CO_2 capacity passed from 2.6 mmol g^{-1} (11.7%) at 25 °C to 0.58 mmol g^{-1} (2.55%) at 100 °C, not so far from the results here obtained for humins foams. However, humins foams have the advantage to be bioderived and sustainable, and that no activation is performed, while MSP-20X is produced from anthracite activated with KOH.

The humins foams could be competitive for CO_2 capture at relevant temperatures, even more if the apparent density of the bed is considered. Tapped density of a powder is calculated as ratio between the mass of the material and the volume it occupies after that has been tapped.

$$\text{Tap density} = \frac{\text{mass}}{\text{tapped volume}}\ (\text{g/mL})$$

Tap density can be seen as the random dense packing. Materials with high surface area generally have a low tap density, and so the needed adsorption volume (column or tank) is higher. For MSP-20X it has been calculated a tap density of 0.35 g cm^{-3}, while we found a much higher tap density of 1.00 g cm^{-3} (Table 7) of grounded F^{2}900 humins foam. Even considering that the MSP-20X of KANSAI Coke adsorbs 2.55 wt.% of CO_2 at 100 °C, compared to 1.17% for F^{2}900 we will need a taller column of MSP-20X because the bed density is much lower (2.9 times). Therefore, humins foams can compete in such applications.

Table 8
Yield and morphological characterization of activated carbon monoliths prepared from F²900 humins foam at 900 °C, using CO_2 flow = 60 mL/min for 10, 20, 40 and 60 min.

Time (min)	Burn off (%)	S_{BET} (m^2/g)	S_{NLDFT} (m^2/g)	$V_{DR\text{-}N2}$ (cm^3/g)	$V_{DR\text{-}CO2}$ (cm^3/g)	V_{NLDFT} (cm^3/g)	$V_{0.97}$ (cm^3/g)	V_{meso} (cm^3/g)
10	14.2	985	1151	0.37	0.33	0.40	0.41	0.01(3%)
20	36	1347	1326	0.49	0.34	0.52	0.56	0.04 (8%)
40	94.8	1482	1289	0.52	0.30	0.56	0.68	0.12 (19%)
60	100	–	–	–	–	–	–	–

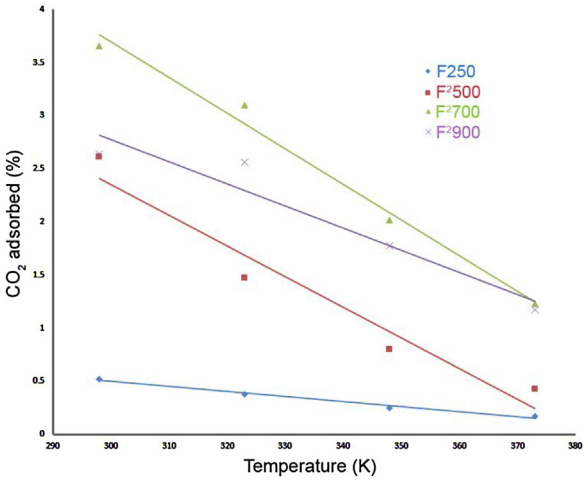

Fig. 7. Representation of CO_2 adsorption trend at different temperatures for F250, F²500, F²700 and F²900.

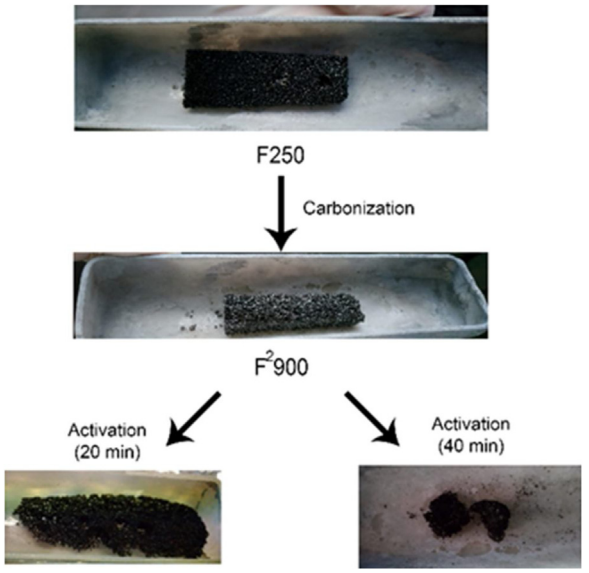

Fig. 8. Activated carbon monoliths produced with 20 and 40 min of CO_2 treatment at 900 °C.

3.6. Activated carbon monoliths preparation

Humins foam F²900 has been used in the preparation of activated carbon with the CO_2 activation technique. Table 8 presents the yields and the main textural parameters obtained by nitrogen and carbon dioxide adsorption, at −196 and 0 °C, respectively, for all the materials tested. The burn-off (loss of material mass) is one of the most important parameters to control in the preparation of activated carbon. As reported by Molina-Sabio et al., in order to maximize the porosity of the material, the burn-off should be less than 40% [74]. Above this amount, although the material is still consumed by CO_2, no higher surface area is reached and, on the contrary, the surface area is increasingly reduced. This occurs because the pores formed during the early stages of activation increase in volume and number, and widen to melt in each other. This, along their external burning, reduces the surface area obtained during the first activation step (Fig. 7).

Table 9
Elemental analysis of activated carbon monoliths. The data are obtained as averages of two replicates.

Sample activation	C/H	%N	%C	%H	%O
10 min	61.46	0.12	90.61	1.47	8.15
20 min	53.72	0.07	86.76	1.61	7.90
40 min	72.96	0.07	76.18	1.05	14.31

The best result was obtained using an activation time of 20 min (Fig. 8), with a burn-off of 36% and a BET surface area of 1347 $m^2\ g^{-1}$. Increasing the activation time to 40 min results in an almost complete loss of material, with a yield of only 5.2%, while after 60 min the entire sample is completely consumed (Fig. 8). The elemental analysis reported in Table 9 also shows how the CO_2 activation

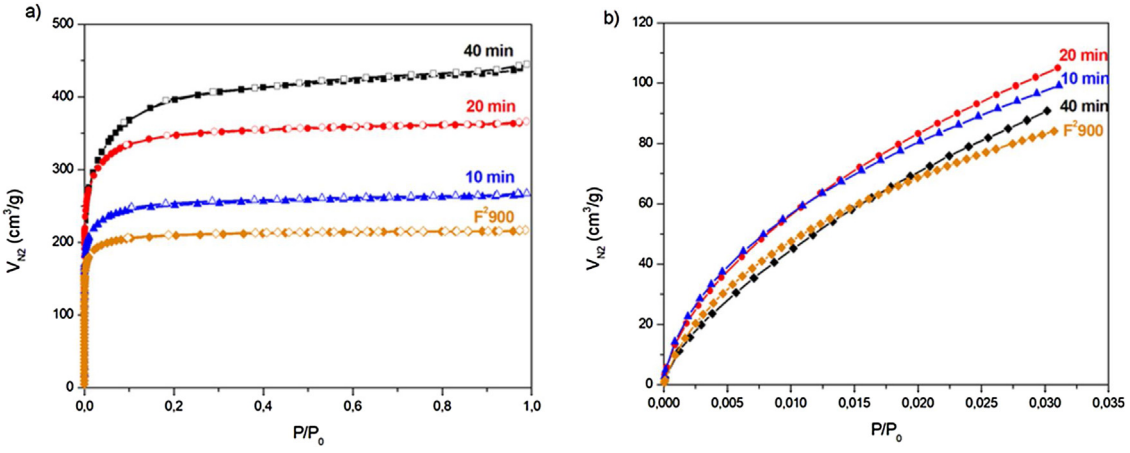

Fig. 9. N_2 adsorption of F²900 and derived activated carbon monoliths produced after 20 and 40 min of CO_2 treatment at 900 °C.

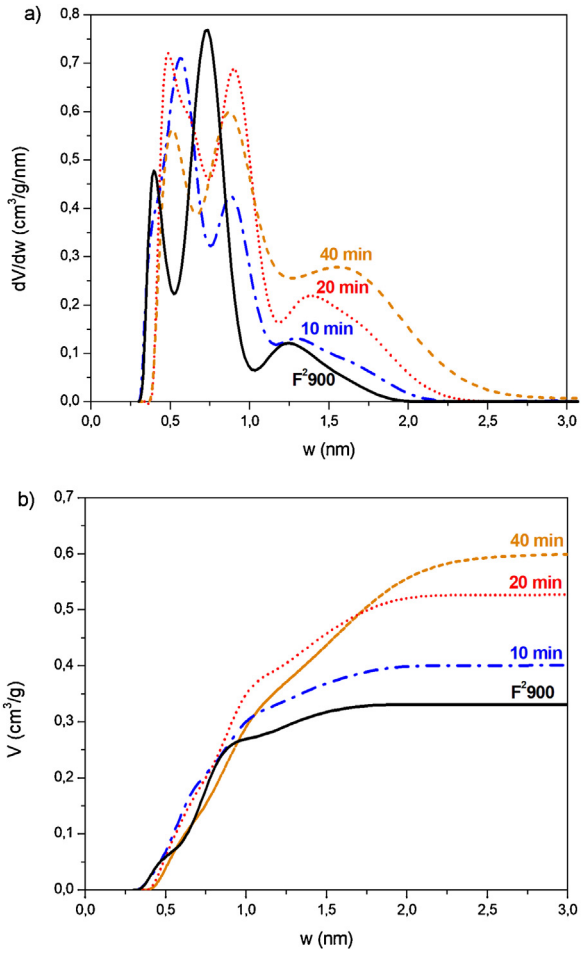

Fig. 10. (a) Pore size distribution and (b) cumulated pore volume calculated by NLDFT.

increases the O % at the expense of C %. This effect is due to the fact that during activation, CO_2 reacts with the carbon of the material, consuming it ($CO_2 + C \rightarrow 2CO$). As a result, C is progressively consumed, and the O/C ratio tends to increase.

F²900 used in these preparations had an O content of 5.60% and a C content of 94.28%. After 10 and 20 minutes of activation, the O % increased by about 30% while the C % decreased by 8%. This effect is even more pronounced after 40 min of activation, where O % reaches 14.31%.

The BET area increased with activation time as well as the porosity in the range of micro and mesopores. Fig. 9 shows the adsorption isotherms of nitrogen (Fig. 9a) and carbon dioxide adsorption (Fig. 9b) on non-activated F²900 foam and activated carbon foams.

By increasing the activation time, the elbow of nitrogen isotherms was widened, indicating a broadening of the microporosity and the total adsorbed volume was also higher. After 40 min of activation, the plateau was no longer horizontal, but a slight slope appeared, indicating the existence of mesoporosity (pores wider than 2 nm) as well as microporosity (pores narrower than 2 nm). The CO_2 adsorption isotherms give an indication of the volume of pores narrower than 1.2 nm. Activation times of up to 20 min created new pores, narrower than 1.2 nm, but higher activation times simply produced pore widening. Thus, the adsorption of CO_2 decreased and that of N_2 adsorption continued to increase. The latter was confirmed by the pore size distribution (PSD) and the cumulative pore volume (Fig. 10) calculated by the NLDFT model.

4. Conclusions

In this work, new materials called humins foams have been prepared from highly viscous humins derived from the industrial acid catalyzed dehydration of fructose into methoxymethylfurfural.

The humins foams were characterized in terms of composition, surface functionality, porosity, and thermal and chemical stability. The carbon content of humins foams can be controlled via the synthesis protocol, and can be as high as 95.4% in the case of carbonization at 900 °C. This makes carbonized humins foams interesting for applications such as electrodes for energy storage and conversion, as catalyst supports, or as cheap adsorbents.

The surface chemistry of several humins foams has been investigated. Foams prepared at a temperature of 180 °C exhibit poor chemical stability, releasing furanic compounds in solution. These furanics might be unbound species present in the mixture of crude humins and originate from an incomplete crosslinking, or come from the hydrolysis of the humins foams structure. Total solvent stability was obtained with foams prepared at temperatures above 250 °C. Of the foams tested, those prepared under air at a temperature below 300 °C had a net negative surface charge in water, with an impressive value of pH of zero point charge of about 2 (while commercial products range between 4 and 10.5). Thanks to this low value of pH of zero point change associated with a cation-exchange capacity, these humins foams can be applied in several fields (e.g. water depollution). In addition, thanks to their rigid and crosslinked nature, they can be prepared in blocks of indefinite dimensions (limited only by the dimensions of the crucible and the oven) and used as a whole. This aspect, as well as the cost efficiency of the crude humins, might be useful for preparing materials for the decontamination of large volumes of solvents, for which a high surface area is required. In contrast with commercially available carbon-materials used for decontamination (mainly based on modified activated carbon) these results are referred to the bare carbon support, where any further activation strategy was applied. In order to enhance the materials properties and make humins foams useful in the adsorption of cationic contaminant, further studies should be conducted, aimed to the enhancement of the surface area (where for commercial products ranges between 500 and 2000 $m^2\ g^{-1}$) and increasing the density of charge on the surface. Treatments with acids, bases or oxidizing agents are often used for modifying chemical and physical properties of carbon materials, and should be tested and screened also for humins foams. Again, the big advantage of humins foams is the three-dimensional starting structure, that can be maintained in the final treated material, while commercial products are generally in form of powder.

Humins foams also have high thermal resistance, which increases with the temperature of preparation. According to headspaces analysis, all the foams tested released only a small amount of degradation gas over a period of 2 h, thus excluding the risks of toxicity in the event of accidental presence of heat sources. The maximum amount of gas released was about 8.5% of the total mass of the sample, obtained by heat treatment of F180 for 2 h at 250 °C. F250 presented a higher thermal resistance, with only 0.43% of mass loss over 2 h. Therefore, according to the data reported here, humins foams prepared at a temperature above 250 °C exhibit the highest thermal and chemical stability, unlike those prepared at a lower crosslinking temperature. F250 also has the lowest thermal conductivity (0.04 $W\ m^{-1}\ K^{-1}$). Considering commercial thermal insulants such as the rigid polyurethane foams, which show lower thermal conductivity (18–28 $W\ m^{-1}\ K^{-1}$) and also lower thermal resistance compared to humins foams, it paves the way for new investigations as insulation material provided of further adjustment. In these terms, by changing the nature of the gas in the humins foams cells, we can increase the elas-

ticity of the material or further reduce the pores size (by foams preparation under pressurized environment) as key steps for future studies

Humins foams have also been tested for CO_2 adsorption at temperatures $\geq$25 °C. The best results have been obtained at 25 °C, whereas the efficiency decreases with the increase of the adsorption temperature tested. Humins foams carbonized at 500 °C showed the fastest adsorption rate at 25 °C, reaching saturation with 2.61 wt.% of CO_2 fixed to the surface after only 37 min of treatment. Moreover, the largest amount of CO_2 adsorbed, 3.66 wt.%, was observed at 25 °C for foams carbonized at 700 °C, while the saturation was reached after 44 min of treatment. Considering the lack of similar studies in literature, further investigations should be performed, while a new application field could be explored.

Finally, the preparation of activated carbon monoliths from humins foams was tested. Physical (CO_2) activation was carried out at 900 °C, reaching a BET surface area of up to 1482 $m^2 g^{-1}$. The best results were obtained after 20 min of treatment, reaching a surface area of 1347 $m^2 g^{-1}$ with only 36% burn-off. These results are way better than those reported in literature for preparations from humins, and are more time and cost effective. Furthermore, the surface area obtained is competitive with those of activated carbon commercially available. The textural characterization showed the presence of meso- and microporosity, as well as pores narrower than 1.2 nm. These activated carbons can compete with those commercially available, with the advantage of great adaptability, because they can be produced in the form of monoliths (easier to handle and recover), and with a favorable cost.

We can assume that all the results reported in this article, referring specifically to humins foams, could be extended (with the necessary limitations) to any material based on thermosetting humins and composites, where viscous crude humins are used as starting material and crosslinked.

Funding

This work has been funded the European Commission for its financial support: H2020 MSCA project “HUGS”, GA 675325.

Authors’ contribution

The manuscript was written by PT and AM and was revised by all the authors. PT and CDS did the foaming preparing experiments. All the other experiments were performed by PT and analyzed by AM. GvK, CH, CL, AC, VF, AM contribute in investigation, conceptualization, design of methodology and validation of results. AM supervised and obtained the funding. All authors have given their approval to the final version of the manuscript.

Conflict of interest

None declared.

Acknowledgements

Special thanks go to Philippe Gadonneix for his help and assistance with elemental analysis and potentiometric titration, and to Blagoj Karakashov for the help with thermal conductivity analysis.

Appendix A. Supplementary data

Supplementary data associated with this article can be found, in the online version, at https://doi.org/10.1016/j.apmt.2020.100622.

References

[1] S.K.R. Patil, C.R.F. Lund, Energy Fuels 25 (2011) 4745–4755.
[2] I. Van Zandvoort, Y. Wang, C.B. Rasrendra, E.R.H. Van Eck, P.C.A. Bruijnincx, H.J. Heeres, B.M. Weckhuysen, ChemSusChem 6 (2013) 1745–1758.
[3] J. Heltzel, S.K.R. Patil, C.R.F. Lund, in: Springer (Ed.), React. Pathways Mech. Thermocatalytic Biomass Convers. II, 2016, pp. 105–118, Singapore.
[4] Z. Cheng, J. Everhart, G. Tsilomelekis, V. Nikolakis, B. Saha, D. Vlachos, Green Chem. 20 (2018) 997–1006.
[5] I. Van Zandvoort, E.J. Koers, M. Weingarth, P.C.A. Bruijnincx, M. Baldus, B.M. Weckhuysen, Green Chem. (2015) 4383–4392.
[6] J. Herzfeld, D. Rand, Y. Matsuki, E. Daviso, M. Mak-jurkauskas, I. Mamajanov, J. Phys. Chem. (2011) 5741–5745.
[8] G.R. Gomes, D.S. Rampon, L.P. Ramos, Appl. Catal. A Gen. 545 (2017) 127–133.
[9] C. Sievers, I. Musin, T. Marzialetti, M.B.V. Olarte, P.K. Agrawal, C.W. Jones, ChemSusChem 2 (2009) 665–671.
[10] S.G. Wettstein, D.M. Alonso, Y. Chong, J.A. Dumesic, Energy Environ. Sci. 5 (2012) 8199–8203.
[11] Y. Román-Leshkov, C.J. Barrett, Z.Y. Liu, J.A. Dumesic, Nature 447 (2007) 982–985.
[12] R.M. Musau, R.M. Munavu, Biomass 13 (1987) 67–74.
[13] C. Moreau, M.N. Belgacem, A. Gandini, Top. Catal. 27 (2004) 11–30.
[14] X. Fang, Z. Wang, B. Yuan, W. Song, S. Li, W. Lin, ChemistrySelect 3 (2018) 12243–12249.
[15] D.W. Rackemann, W.O. Doherty, Biofuels Bioprod. Biorefining 5 (2011) 198–214.
[16] F.S. Asghari, H. Yoshida, Ind. Eng. Chem. Res. 46 (2007) 7703–7710.
[17] M.-M. Titirici, R.J. White, N. Brun, V.L. Budarin, D.S. Su, F. del Monte, J.H. Clark, M.J. MacLachlan, Chem. Soc. Rev. 44 (2015) 250–290.
[18] J. Shen, C.E. Wyman, AIChE J. 58 (2012) 236–246.
[19] B. Girisuta, B. Danon, R. Manurung, L.P.B.M. Janssen, H.J. Heeres, Bioresour. Technol. 99 (2008) 8367–8375.
[20] R. Weingarten, J. Cho, R. Xing, W.C. Conner, G.W. Huber, ChemSusChem 5 (2012) 1280–1290.
[21] B.F.M. Kuster, Carbohydr. Res. 54 (1977) 177–183.
[22] B. Girisuta, L.P.B.M. Janssen, H.J. Heeres, Ind. Eng. Chem. Res. 46 (2007) 1696–1708.
[23] L. Faba, D. Garcés, E. Díaz, S. Ordóñez, ChemSusChem (2019) 1–10.
[24] S. Xu, D. Pan, Y. Wu, N. Xu, H. Yang, L. Gao, W. Li, G. Xiao, Ind. Eng. Chem. Res. 58 (2019) 9276–9285.
[25] Z. Cao, Z. Fan, Y. Chen, M. Li, T. Shen, C. Zhu, H. Ying, Appl. Catal. B Environ. 244 (2019) 170–177.
[26] M.R. Whitaker, A. Parulkar, P. Ranadive, R. Joshi, N.A. Brunelli, ChemSusChem 12 (2019) 2211–2219.
[27] D. Garcés, L. Faba, E. Díaz, S. Ordóñez, ChemSusChem 12 (2019) 924–934.
[28] P. Ramesh, A. Kritikos, G. Tsilomelekis, React. Chem. Eng. 4 (2019) 273–277.
[29] S. Liu, K. Wang, H. Yu, B. Li, S. Yu, Sci. Rep. 9 (2019) 1–9.
[30] A. Mija, J.C. Van Der Waal, J. Pin, N. Guigo, E. De Jong, Constr. Build. Mater. 139 (2016) 594–601.
[31] L. Filiciotto, A.M. Balu, A.A. Romero, E. Rodríguez-Castellón, J.C. van der Waal, R. Luque, Green Chem. 19 (2017) 4423–4434.
[32] S. Kang, G. Zhang, Q. Yang, J. Tu, X. Guo, F.G.F. Qin, Y. Xu, BioResources 11 (2016) 9496–9505.
[33] S. Kang, J. Fu, G. Zhang, W. Zhang, H. Yin, Y. Xu, Polymers (Basel) 9 (2017) 373.
[34] A. Mija, J.C. van der Waal, E. de Jong, G.P.M. van Klink, Process for the modification of humins, WO 2018/062995 A1 (2018).
[35] A. Schweizer, (1940) 781–784.
[36] T.M.C. Hoang, E.R.H. van Eck, W.P. Bula, J.G.E. Gardeniers, L. Lefferts, K. Seshan, Green Chem. 17 (2015) 959–972.
[37] I. van Zandvoort, Towards the Valorization of Humin By-Products: Characterization, Utrecht University, 2015.
[38] A. Sangregorio, N. Guigo, J.C. van der Waal, N. Sbirrazzuoli, ChemSusChem (2018).
[39] X. Montané, R. Dinu, A. Mija, Molecules 24 (2019) 4110.
[40] A. Mija, J.C. van der Waal, G. van Klink, E. de Jong, Humins-containing foam, WO2017074183A8 (2016).
[41] A. Mija, E. de Jong, J.C. van der Waal, G. van Klink, Humins containing foam, WO 2017074183 A1 20170504 (2017).
[42] J.M. Pin, N. Guigo, A. Mija, L. Vincent, N. Sbirrazzuoli, J.C. van der Waal, E. de Jong, ACS Sustain. Chem. Eng. 2 (2014) 2182–2190.
[43] P. Tosi, G.P. van Klink, A. Celzard, V. Fierro, L. Vincent, E. de Jong, A. Mija, ChemSusChem 11 (2018) 2797–2809.
[44] K. Kadirvelu, M. Kavipriya, C. Karthika, M. Radhika, N. Vennilamani, S. Pattabhi, Bioresour. Technol. 87 (2003) 129–132.
[45] N. Mohamad Nor, L.C. Lau, K.T. Lee, A.R. Mohamed, J. Environ. Chem. Eng. 1 (2013) 658–666.
[46] S. Kang, J. Fu, Z. Deng, S. Jiang, G. Zhong, Y. Xu, J. Guo, J. Zhou, Sustainability 10 (2018) 16–19.
[47] D. Chernysheva, Y. Chus, V. Klushin, T. Lastovina, L. Pudova, N. Smirnova, O. Kravchenko, V. Chernyshev, V.P. Ananikov, ChemSusChem 11 (2018) 3599–3608.
[48] H.-P. Boehm, E. Diehl, W. Heck, R. Sappok, Angew. Chem. Int. Ed. English 3 (1964) 669–677.
[49] H.P. Boehm, Carbon N. Y. 32 (1994) 759–769.

[50] S. Brunauer, P.H. Emmett, E. Teller, J. Am. Chem. Soc. 60 (1936) 309–319.
[51] J. Jagiello, C. Ania, J. Parra, C. Cook, Carbon N. Y. 91 (2015) 330–337.
[52] J. Jagiello, J.P. Olivier, Adsorption 19 (2013) 777–783.
[53] J. Jagiello, J. Kenvin, A. Celzard, V. Fierro, Carbon N. Y. 144 (2009) 206–215.
[54] G. Sdanghi, V. Nicolas, K. Mozet, G. Maranzana, A. Celzard, V. Fierro, Int. J. Hydrogen Energy 44 (2019) 16811–16823.
[55] P. Tosi, G.P.M. van Klink, A. Celzard, V. Fierro, L. Vincent, E. de Jong, A. Mija, ChemSusChem 11 (2018) 2797–2809.
[56] J. Encalada, K. Savaram, N.A. Travlou, W. Li, Q. Li, C. Delgado-Sánchez, V. Fierro, A. Celzard, H. He, T.J. Bandosz, ACS Catal. 7 (2017) 7466–7478.
[57] G. Tondi, V. Fierro, A. Pizzi, A. Celzard, Carbon N. Y. 47 (2009) 1480–1492.
[58] W. Zhao, A. Pizzi, V. Fierro, G. Du, A. Celzard, Mater. Chem. Phys. 122 (2010) 175–182.
[59] F.I. Morais, A.L. Page, L.J. Lund, Soil Sci. Soc. Am. J. 40 (1976) 521–527.
[60] J. Rivera-Utrilla, I. Bautista-Toledo, M.A. Ferro-Garca, C. Moreno-Castilla, J. Chem. Technol. Biotechnol. 76 (2001) 1209–1215.
[61] P.C.C. Faria, J.J.M. Órfão, M.F.R. Pereira, Water Res. 38 (2004) 2043–2052.
[62] J.S. Noh, J.A. Schwarz, J. Colloid Interface Sci. 130 (1989) 157–164.
[63] S. Žalac, N. Kallay, J. Colloid Interface Sci. 149 (1992) 233–240.
[64] H.-P.H. Boehm, Carbon N. Y. 40 (2002) 145–149.
[65] H.P. Boehm, Adv. Catal. 16 (1966) 179–274.
[66] A. Contescu, C. Contescu, K. Putyera, J.A. Schwarz, Carbon N. Y. 35 (1997) 83–94.
[67] S.L. Goertzen, K.D. Thériault, A.M. Oickle, A.C. Tarasuk, H.A. Andreas, Carbon N. Y. 48 (2010) 1252–1261.
[68] I.I. Salame, T.J. Bandosz, J. Colloid Interface Sci. 240 (2001) 252–258.
[69] Bing, in: F. of E.R.P.F. Associations (Ed.), Rep. N1, Federation of European Rigid Polyurethane Foam Associations, 2006, pp. 1–33.
[70] A. Muralidhara, A.R. Division, I. National, D. Environnement, Biofuels Bioprod. Biorefining (2019) 464–470.
[71] A. Muralidhara, P. Tosi, A. Mija, N. Sbirrazzuoli, C. Len, V. Engelen, E. de Jong, G. Marlair, ACS Sustain. Chem. Eng. (2018) 16692–16701.
[72] E.S. Sanz-Pérez, M. Olivares-Marín, A. Arencibia, R. Sanz, G. Calleja, M.M. Maroto-Valer, Int. J. Greenh. Gas Control 17 (2013) 366–375.
[73] V. Fierro, E. García-Díez, S. Schaefer, A. Sanchez-Sanchez, M.M. Maroto-Valer, S. García, A. Celzard, Carbon2019, Lexington, USA, 2019.
[74] M. Molina-Sabio, M.T. González, F. Rodriguez-Reinoso, A. Sepúlveda-Escribano, Carbon N. Y. 34 (1996) 505–509.